ISSN 1453 – 7303 **"HIDRAULICA" (No. 4/2025)**
Magazine *of Hydraulics, Pneumatics, Tribology, Ecology, Sensorics, Mechatronics*

Green Infrastructure Solutions for Urban Flood Risk Mitigation in Secondary Streets

Dr. **Maritza ARGANIS**[1,2,*], M. Eng. Margarita **PRECIADO**[3,*],
Eng. José Enrique **GUTIERREZ-SANCHEZ**[3]

[1] Universidad Nacional Autónoma de México. Instituto de Ingeniería. México

[2] Universidad Nacional Autónoma de México. Facultad de Ingeniería. México

[3] Mexican Institute of Water Technology. México

* MArganisJ@iingen.unam.mx; preciado@tlaloc.imta.mx

Abstract: *Urban flooding remains a major issue in densely populated cities, where conventional drainage systems often fail under extreme rainfall. This study uses 2D Saint-Venant hydrodynamic modelling to evaluate the impact of Green Infrastructure (GI) on surface runoff in secondary urban streets. Four scenarios were simulated, from fully impervious surfaces to layouts with vegetated strips and rain gardens. Results show that increasing vegetated area and surface roughness can reduce peak flow by up to 31%, velocity by 38%, and inundation extent by 42%, while delaying peak time by up to seven minutes. These findings highlight the hydraulic benefits of GI in enhancing urban flood resilience and pedestrian safety. The modelling framework supports the integration of Nature-Based Solutions into urban water management strategies.*

Keywords: *Green infrastructure (GI), urban flood resilience, Saint-Venant equations, nature-based solutions (NbS)*

1. Introduction

Two-dimensional (2D) hydrodynamic modelling has become a cornerstone in analysing surface flow dynamics within urban environments. Recent studies have applied these models across diverse domains—from risk management and infrastructure design to climate resilience and urban planning. Urban flood modelling requires either data-intensive, computationally heavy 1D-2D coupled models or highly simplified equivalent drainage schemes. To bridge this gap, a manhole-based equivalent drainage model has been proposed, which improves accuracy and efficiency by explicitly defining manholes as the drainage locations and calculating dynamic displacement volumes [1].
Into flood risk context, Alcocer-Yamanaka et al. (2016) [2] and Mark et al. (2025) [3] leveraged 2D simulations to assess urban vulnerability and calibrate flood models using historical data. Infrastructure-focused research by [4] Korgaonkar et al. (2019) and Onur (2024) [5] explored vegetated streets and rain gardens, demonstrating their role in runoff attenuation. Meanwhile, Enriquez de Salamanca (2020) [6] and Sim and Kim (2024) [7] emphasized the importance of spatial and temporal resolution when modeling extreme rainfall events in dense urban areas.
Integrative approaches, such as those by Sinagra et al. (2022) [8] and Ali et al. (2025) [9], combined hydrodynamic modelling with GIS to identify flood-prone zones and propose green infrastructure (GI) interventions, with a review of the technical, social, and economic challenges. Horrit and Bates. (2002) [10] evaluate the accuracy and applicability of each modelling approach under different conditions. Their findings show that while 1D models are computationally efficient, 2D models provide more detailed spatial representations of flood extents, especially in complex urban terrains, making them more suitable for high-resolution flood risk assessments. To address the intensified hydrological response of urban landscapes, Nature-Based Solutions (NbS)—particularly GI—have emerged as multifunctional strategies for stormwater management and climate adaptation. Vegetated strips, rain gardens, and bioretention zones offer ecosystem services including microclimate regulation, water quality enhancement, and significant runoff reduction [11-14].

Effective stormwater management through Green Infrastructure (GI) requires a multi-scale decision process that integrates site-specific biophysical conditions with the broader urban water system and pollution sources. This includes specialized guidance, such as that developed for cities like Detroit and Addis Ababa, to address distinct regional challenges like combined sewer overflows versus seasonal flooding and untreated discharge [15].
This research contributes to the global discourse on urban flood resilience by applying hyper-resolution 2D Saint-Venant simulations to secondary street networks—an often-overlooked scale in conventional flood modelling [16,17]. The novelty lies in the rigorous integration of GI into stormwater modelling and the local-scale quantification of its performance.

2. Methodology

A 2D Saint-Venant model was implemented, selected for its robust handling of shallow urban flows and its compatibility with high-resolution raster inputs. The model domain was discretized at 0.5-meter resolution to capture microtopographic features critical to flow behaviour in narrow urban corridors.

2.1 Saint-Venant equations

Simulation is based on the two-dimensional Saint-Venant equations, which describe surface flow in terms of mass and momentum conservation [18-22].
Continuity:

$$\partial h/\partial t + \partial(uh)/\partial x + \partial(vh)/\partial y = R - I \tag{1}$$

Momentum in x-direction:

$$\partial(uh)/\partial t + \partial(u^2h + 0.5gh^2)/\partial x + \partial(uvh)/\partial y = -gh\partial z/\partial x - \tau x/\rho \tag{2}$$

Momentum in y-direction:

$$\partial(vh)/\partial t + \partial(uvh)/\partial x + \partial(v^2h + 0.5gh^2)/\partial y = -gh\partial z/\partial y - \tau y/\rho \tag{3}$$

Where:
h is water depth, u and v are velocities in x and y directions g is gravitational local acceleration, z is terrain elevation, τx and τy are shear stresses, ρ is water density, R is rainfall, and I is infiltration.

2.2 Green infrastructure and drainage elements

This model incorporates green surfaces such as vegetated strips between traffic lanes, medians, and sidewalks. These areas help reduce flow velocity and increase infiltration. According to [23] Jabbar et al. (2022), urban green areas provide ecosystem services such as microclimate regulation, runoff reduction, and air quality improvement. Magaña Rodríguez et al. (2021) [24] emphasize that green infrastructure can be integrated into urban design to mitigate climate risks and enhance city resilience. Drainage elements include stormwater grates and manholes. Fuentes-Mariles et al. (2023) [25] propose optimized designs for urban drainage networks using strategically connected manholes to minimize travel distances and costs. Typical rates in Mexico measure 0.6 m × 0.6 m, while manholes are cylindrical structures with a 1.2 m diameter and up to 3 m depth.
Retaining necessity, the full momentum terms is directly related to quantifying the mitigation Green Infrastructure performance. The primary mechanism by which vegetated areas reduce peak flow is through hydraulic resistance, functioning as a momentum sink. This physical interaction is explicitly captured by the bed shear stress terms (τx,τy), which are calculated based on Manning's roughness coefficient (n). By assigning a significantly higher *n* value to vegetated zones compared to asphalt (n considered within 0.015-0.03), the model simulates a drastic loss of flow momentum, causing rapid deceleration near the GI areas. This momentum dissipation increases the water residence time, which in turn enhances the opportunity for infiltration to occur. If a simplified model lacking these dynamic terms were used, the resulting ability to accurately simulate the combined hydraulic and hydrological impact of GI would be fundamentally compromised.

The simulations were performed using a two-dimensional Saint-Venant model with rainfall input based on the September 28, 2025 storm. Four scenarios were analysed (Figures 1 and 2):

1. No green zones.
2. Two small green zones (1m × 1m, Manning n = 0.1).
3. Four medium green zones (2m × 2m, Manning n = 0.2).
4. Ten large green zones (2m × 2m, Manning n = 0.2) distributed along both sides of the street.

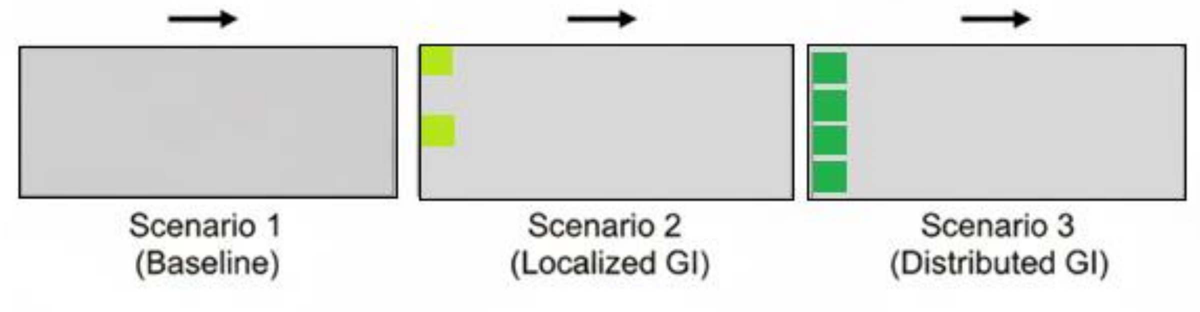

Fig. 1. Tested Scenarios 1 to 3

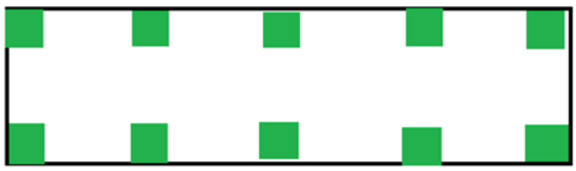

Fig. 2. Tested Scenario 4. Own design with the help of an AI Designer

2.3 Dual-drainage representation and sink terms

Urban flood risk complete analysis often involves dual drainage modelling, which couples the 1D subsurface sewer network dynamics with the 2D overland flow hydrodynamics. This approach allows for the simulation of complex interactions, such as water entering the sewer system through grates and, critically, water surcharging from overloaded manholes onto the surface [26-28]. In this specific 2D surface flow investigation, the complexity of dynamic 1D/2D coupling is avoided to focus purely on the surface mitigation provided by the GI. The effect of the subsurface drainage system is simplified by representing drainage elements—such as stormwater grates and manholes—as localized sink terms in the 2D domain. These drainage points remove water from the surface based on flow depth and engineered capacity [1]. Typical urban drainage infrastructure in Mexico includes grates measuring 0.6 m × 0.6 m and manholes with a 1.2 m diameter. The sink term functions as a fixed boundary condition for water removal.

While this approach is acceptable for focusing on surface runoff mitigation, it is a necessary limitation. If the goal were to simulate extreme events where flooding is caused by sewer overload or pressure head lifting manhole covers, a full 1D/2D coupled framework (such as Iber-SWMM or InfoWorks ICM) would be required [7], [29]. For hyper-resolution simulation over large urban catchments (approximately 40 km²), advanced coupled models utilizing hybrid parallelization techniques, such as the H12 code, are necessary to maintain computational efficiency while accurately capturing the dual drainage process [30].

2.4 Simulation program

The simulation program utilizes a computational approach to model surface flow in urban streets. This program is designed to integrate different surface types, such as those with grass or roots, by assigning distinct Manning roughness values. Figure 3 illustrates a flowchart that shows the steps performed by the methodology.

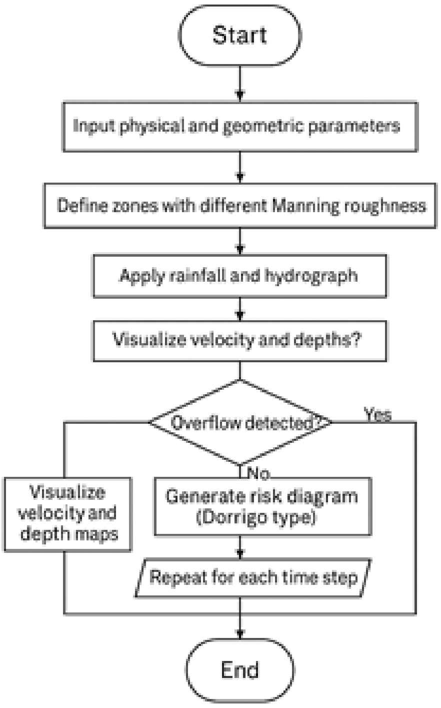

Fig. 3. Methodology Flowchart. Source: Own design with the help of an AI Designer

2.5 Study area

The computational domain for this simulation is a 20 m × 100 m street segment (Figure 4), representative of a secondary street network susceptible to pluvial flooding in a high-density urban environment (Figure 4). The geometry includes realistic features such as traffic lanes, curbs, and sidewalk areas. Accurate surface flow modelling necessitates high-resolution topographic input. The digital terrain model (DEM) used must be derived from high-fidelity data, such as LiDAR, post-processed to a fine grid resolution to correctly represent micro-topography, including subtle changes in elevation, curb heights, and the precise geometric placement of GI installations. These fine details are crucial as they determine the initial path of shallow flow and define areas of ponding.

Figure 5 shows the hyetograph assumed in the simulations (high intensity storm), an entry hydrograph to the street was assumed equal to zero and Table 1 contains the data of the hypothetical example used for all simulations.

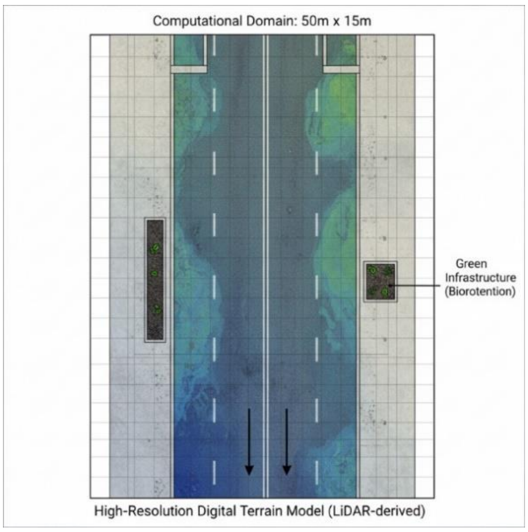

Fig. 4. Computational Domain Street. Own design with the help of an AI Designer

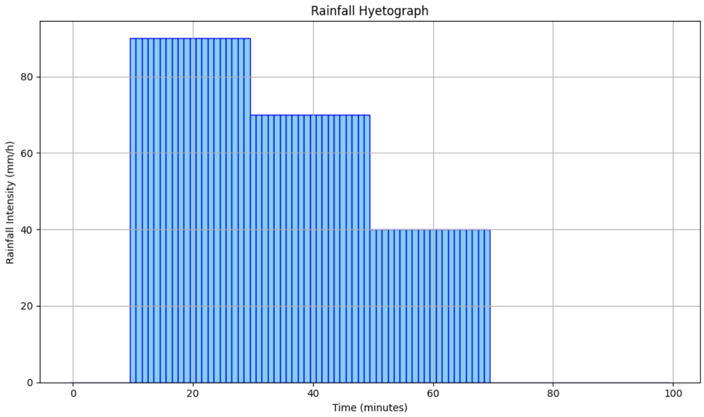

Fig. 5. Hyetograph used in the simulations

Table 1: Data set

Parameter	Unit	Value	Description
Street length	m	100	Total length of the modeled urban street
Street width	m	20	Total width of the modeled urban street
Curb height	m	0.5	Vertical distance between the street surface and the top of the sidewalk
Cell size in X	m	1	Grid resolution in the X direction
Cell size in Y	m	1	Grid resolution in the Y direction
Time step	s	0.1	Temporal resolution of the simulation
Number of time steps	–	100	Total number of simulation steps
Initial water depth	m	0.001	Starting water depth across the domain
Initial velocity in X	m/s	0	Initial flow velocity in the X direction
Initial velocity in Y	m/s	0	Initial flow velocity in the Y direction
Gravitational acceleration	m/s^2	9.81	Standard gravity constant
Manning's roughness coefficient (n)	–	0.03	Surface roughness for the street
Ks (saturated hydraulic conductivity)	m/s	0	No infiltration considered in this example
Suction	m	0	Soil suction head (not active in this case)
Moisture deficit	–	0	Initial soil moisture deficit (no infiltration)

3. Results and discussion

Simulation results show a consistent trend of hydrological improvement as the number and size of vegetated areas increase. In all GI configurations, flow attenuation and infiltration were evident, particularly near vegetated zones with elevated Manning roughness coefficients. Peak flow reduction ranged from 18% in localized vegetated strips to over 30% in distributed GI layouts. Correspondingly, maximum velocity reductions of up to 39% were observed, indicating enhanced flow resistance and localized energy dissipation.
Rain gardens produced the most substantial improvements, reflecting their greater storage and infiltration capacity compared to shallow vegetated strips. These physical processes resulted in notable hydraulic benefits: the total flooded area decreased from 1,240 m² under impervious conditions to just 720 m² with rain garden integration. Spatial flood maps illustrated this transformation, revealing a marked contraction of inundation extents and a transition from high- to moderate-risk zones.

3.1 Simulation maps

Figures 6 to 9 illustrate the spatial distribution of maximum water depths and flow velocities obtained from the four simulation scenarios. These maps highlight how the presence, size, and arrangement of vegetated areas influence surface flow dynamics within the modelled street segment.
In the baseline scenario (Figure 6), the absence of green zones results in higher flow concentration along the central axis of the street, producing maximum velocities exceeding 1.5 m/s and depths greater than 0.30 m in localized depressions. This configuration reflects the typical response of an impervious urban surface where runoff moves rapidly toward low-lying areas, increasing flood and safety risks.

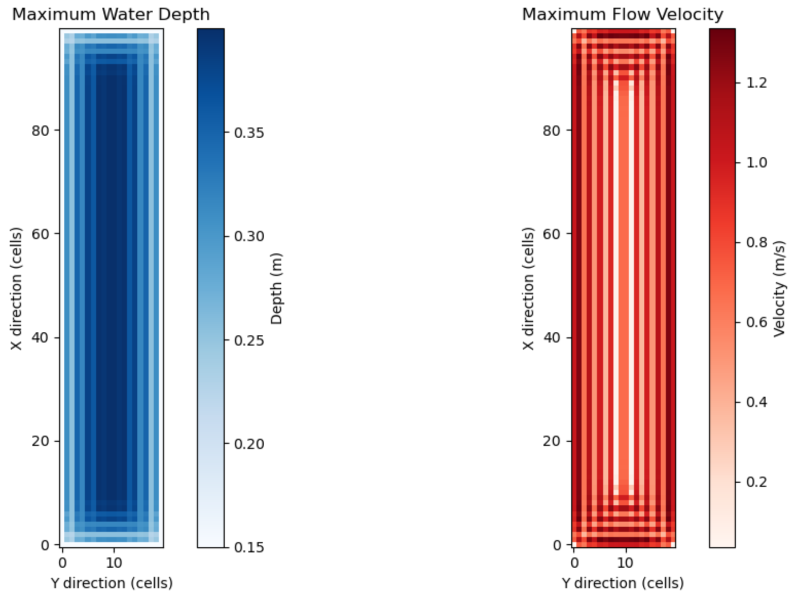

Fig. 6. Maximum Depth and Velocity Map – Simulation No green zones

The two small green zones' introduction (Figure 7) yields a moderate reduction in flow velocity around the vegetated surfaces, indicating localized hydraulic resistance. However, high-velocity cores remain visible in the central street sector, suggesting limited overall attenuation at this scale.

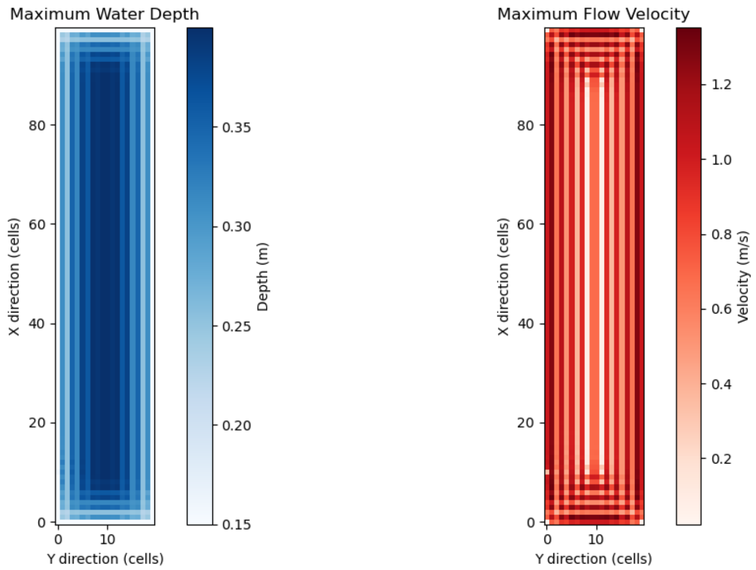

Fig. 7. Maximum Depth and Velocity Map - Simulation 2 – Two 1x1 m green zones with Manning n = 0.1

When four larger green zones are incorporated (Figure 8), the reduction in both depth and velocity becomes more pronounced. Flow deceleration and redistribution are observed along the vegetated areas, creating partial barriers that promote temporary ponding and enhance infiltration. Consequently, high-risk zones contract significantly compared to the previous configurations.

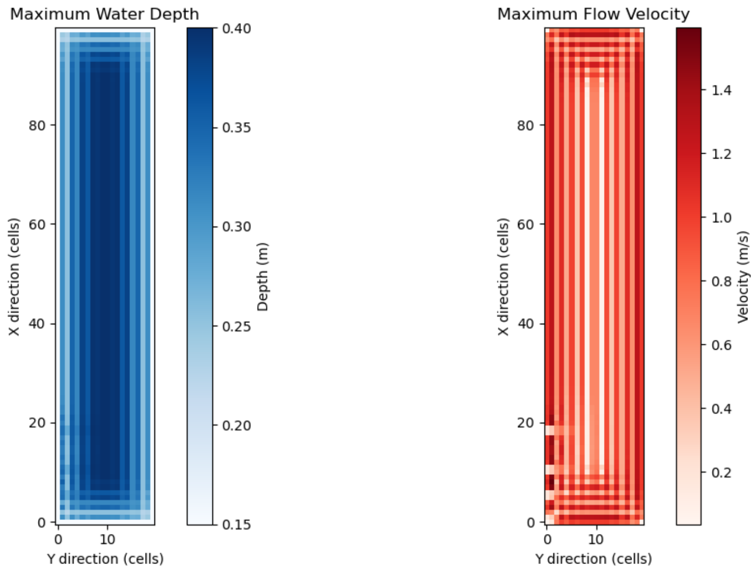

Fig. 8. Maximum Depth and Velocity Map - Simulation 3 – Four 2x2 m green zones with Manning n = 0.2

Finally, the distributed green infrastructure scenario (Figure 9) demonstrates the most substantial improvements. The ten 2 × 2 m vegetated patches along both street sides generate widespread velocity attenuation and uniform depth reduction. This configuration minimizes critical flow pathways and nearly eliminates continuous high-velocity zones, providing the most stable and hydraulically balanced condition among all simulations. These spatial results confirm that distributed vegetation produces cumulative benefits, not only reducing local peak velocities but also improving the overall hydraulic behaviour of the street. By enhancing flow resistance and promoting infiltration, strategically placed GI elements transform secondary streets into effective components of urban flood mitigation systems.

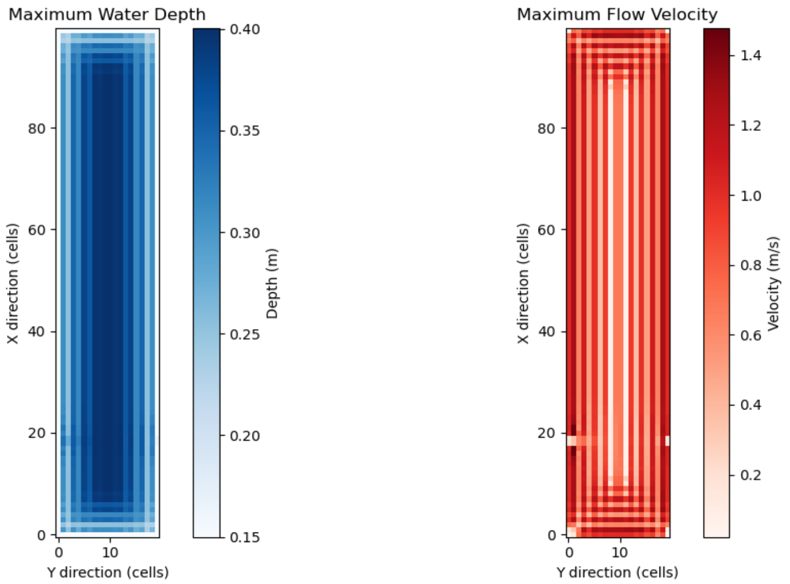

Fig. 9. Maximum Depth and Velocity Map - Simulation 4 – Ten 2x2 m green zones distributed along both sides

Although all simulations recorded 236 border cells with overflow, the green infrastructure (GI) inclusion elements significantly altered the surface flow dynamics. The main effects observed were:
Reduction in flow velocity as a direct result of increased surface roughness in vegetated areas.
Attenuation of water depth in critical zones due to localized infiltration and momentum loss.
Decreased overturning risk for pedestrians, particularly evident in the fourth scenario featuring distributed vegetation.
These outcomes are especially relevant for streets lacking conventional drainage systems, where GI acts as a passive yet effective flood mitigation mechanism.

3.2 Dorrigo risk diagram and temporal analysis

The temporal analysis further emphasized the functional benefits of GI implementation. The distributed vegetation configuration delayed the time to peak discharge by up to seven minutes, effectively providing additional buffering capacity during intense rainfall events. This delay reduces hydraulic pressure on downstream drainage infrastructure and mitigates the potential for compound flooding.
From a pedestrian safety perspective, the Dorrigo risk analysis revealed a marked reduction in overturning risk zones. In the distributed vegetation scenario, areas where the product of depth × velocity exceeded the 0.42 m^2/s threshold were substantially diminished. This demonstrates the GI dual benefits in enhancing both hydraulic performance and public safety during flood events.
Overall, these results confirm that the spatial configuration and hydraulic design of green infrastructure strongly determine its effectiveness. While all scenarios improved flow behavior relative to the baseline, the distributed vegetation layout produced the most balanced outcomes—combining significant reductions in runoff and flow velocity with increased time-to-peak and enhanced pedestrian safety. These findings highlight the potential of micro-scale GI deployment in local street networks as a scalable strategy to strengthen city-wide flood resilience.
The Dorrigo Risk Diagram presented in Figure 10 illustrates the overturning risk threshold for adults, defined by the product of flow depth and velocity exceeding 0.42 m^2/s, corresponding to the onset of unstable footing in flooded conditions.

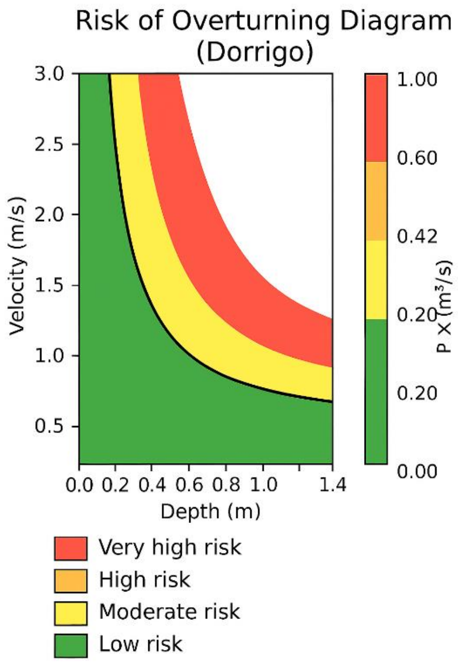

Fig. 10. Risk of overturning map (Dorrigo). Results by Simulation for Maximum Depth and Velocity Values.
Source: Own design with the help of an AI Designer

Simulation 1 (without green zones or drainage):

• Zones with depth > 0.3 m and velocity > 1.5 m/s are observed in the centre of the street.

🔴 Very high overturning risk zones: between rows 40–60 and columns 8–12.

🟠 High-risk zones: extended toward the lateral edges.

Simulation 2 (2 small green zones):

• Green zones slightly reduce velocity in their surroundings.

🔴 Very high risk: still present in the centre, but more localized (rows 45–55, columns 9–11).

🟠 High risk: more dispersed than in Simulation 1.

Simulation 3 (4 large green zones):

• Greater velocity reduction is observed in the green zones.

🔴 Very high risk: only in small areas between green zones (rows 48–52, columns 10–12).

🟡 Moderate risk: at the edges of the green zones.

Simulation 4 (10 distributed green zones):

• Distributed vegetation significantly reduces the risk.

🟠 High risk: only in isolated points (rows 50–55, columns 9–10).

🟢 Most of the street is in low or moderate risk.

From these results is noticed that green zones have a clear effect in reducing overturning risk, especially when strategically distributed. Simulation 4 is the safest in terms of overturning risk. Zones with very high risk should be prioritized for intervention (drainage works, vegetation, signage).

4. Conclusions

This paper demonstrates that Green Infrastructure (GI) represents an effective, low-impact strategy for mitigating urban flood risk in secondary streets, which often remain overlooked in conventional drainage planning. Integrating vegetated zones into existing asphalt surfaces significantly reduces flow velocity, runoff volume, and flood extent, while simultaneously improving pedestrian safety and enhancing the overall hydraulic resilience of the urban environment.

Although the total overflow cell count remained unchanged across scenarios, the redistribution of flow energy and delay in time to peak discharge confirm the hydraulic efficiency of GI systems under intense rainfall conditions. These outcomes highlight the ability of vegetated features to moderate hydrodynamic forces and stabilize flow patterns in highly impervious areas.

Among the evaluated configurations, distributed vegetation provided the most robust performance. By increasing surface roughness, it induced energy dissipation and promoted localized infiltration, producing a balanced reduction in both depth and velocity throughout the modelled domain. Beyond their hydraulic role, these vegetated systems contribute to ecosystem restoration, microclimate regulation, and urban aesthetic enhancement, aligning with broader climate adaptation and sustainability objectives.

The high-resolution 2D Saint-Venant modelling framework employed in this research offers a valuable methodological reference for urban planners and engineers. It enables the precise assessment of GI performance at the street scale and supports evidence-based decision-making for retrofitting or designing stormwater infrastructure. Municipalities can apply this approach to prioritize cost-effective, nature-based interventions that deliver measurable hydraulic benefits while co-generating social and environmental value.

In accordance with the above, strategically designed and spatially distributed GI systems transform secondary streets into multifunctional hydrological assets. Their implementation not only mitigates local flooding and improves public safety but also strengthens the adaptive capacity of cities facing more frequent and intense rainfall events. By embracing these nature-based solutions, urban areas can evolve toward safer, greener, and more resilient futures.

References

[1] Xiang, M., S. Zhang, C. Wu, and C. Tang. "A Two-Dimensional Hydrodynamic Urban Flood Model Based on Equivalent Drainage of Manholes." *Journal of Hydroinformatics* 26, no. 2 (2024): 519–533. https://doi.org/10.2166/hydro.2024.240.

[2] Alcocer-Yamanaka, V. H., J. M. Rodríguez-Varela, V. J. Bourguett-Ortiz, O. J. Llaguno-Guilberto, and P. M. Albornoz-Góngora. " Methodology for generating flood risk maps in urban areas / Metodología para la generación de mapas de riesgo por inundación en zonas urbanas." *Tecnología y Ciencias del Agua* 7, no. 5 (2016): 33–55. https://dialnet.unirioja.es/servlet/articulo?codigo=7357119.

[3] Mark, O., J. Hénonin, N. D. S. Domingo, B. Russo, A. S. Chen, and S. Djordjević. "Report and Papers with Guidelines on Calibration of Urban Flood Models." University of Exeter Repository, 2025. https://ore.exeter.ac.uk/articles/report/Report_and_papers_with_guidelines_on_calibration_of_urban_flood_models/29718473.

[4] Korgaonkar, Y., D. P. Guertin, D. C. Goodrich, C. Unkrich, W. G. Kepner, and I. S. Burns. "Modeling Urban Hydrology and Green Infrastructure Using the AGWA Urban Tool and the KINEROS2 Model." *Frontiers in Built Environment* 4 (2018): 58. https://doi.org/10.3389/fbuil.2018.00058.

[5] Onur, M. "The Employment of Rain Gardens in Urban Water Management to Improve Biodiversity and Ecosystem Resilience." In *Nature-based Solutions for Circular Management of Urban Water*, 73–91. Springer, 2024. https://doi.org/10.1007/978-3-031-50725-0_5.

[6] Enríquez-de-Salamanca, Á. "Victims Crossing Overflowing Watercourses with Vehicles in Spain." *Journal of Flood Risk Management* 13, no. 4 (2020): e12645. https://doi.org/10.1111/jfr3.12645.

[7] Sim, S.-B., and H.-J. Kim. "An Urban Flood Model Development Coupling the 1D and 2D Model with Fixed-Time Synchronization." *Water* 16, no. 19 (2024): 2726. https://doi.org/10.3390/w16192726.

[8] Sinagra, M., C. Nasello, and T. Tucciarelli. "Urban Flood Prediction Through GIS-Based Dual-Coupled Hydraulic Models." *Hydrology* 9, no. 10 (2022): 174. https://doi.org/10.3390/hydrology9100174.
[9] Ali, L., S. Gato-Trinidad, and M. Imteaz. "Green Infrastructure and Urban Flooding: A Survey of Prevailing Issues and Current Modelling Approaches." *Water Resources Management* 39 (2025): 3697–3714. https://doi.org/10.1007/s11269-025-04125-6.
[10] Horritt, M. S., and P. D. Bates. "Evaluation of 1D and 2D Numerical Models for Predicting Flood Inundation." *Journal of Hydrology* 268, no. 1–4 (2002): 87–99. https://doi.org/10.1016/S0022-1694(02)00121-X.
[11] Meerow, S., and J. P. Newell. "Spatial Planning for Multifunctional Green Infrastructure: Growing Resilience in Detroit." *Landscape and Urban Planning* 159 (2017): 62–75. https://doi.org/10.1016/j.landurbplan.2016.10.005.
[12] Fletcher, T. D., W. Shuster, W. F. Hunt, R. Ashley, D. Butler, S. Arthur, S. Trowsdale, S. Barraud, A. Semadeni-Davies, J.-L. Bertrand-Krajewski, P. S. Mikkelsen, G. Rivard, M. Uhl, D. Dagenais, and M. Viklander. "SUDS, LID, BMPs, WSUD and More – The Evolution and Application of Terminology Surrounding Urban Drainage." *Urban Water Journal* 12, no. 7 (2015): 525–542. https://doi.org/10.1080/1573062X.2014.916314.
[13] Li, C., T. D. Fletcher, H. P. Duncan, and M. J. Burns. "Can Stormwater Control Measures Restore Altered Urban Flow Regimes at the Catchment Scale?" *Journal of Hydrology* 549 (2017): 631-653. https://doi.org/10.1016/j.jhydrol.2017.03.037.
[14] Demuzere, M., K. Orru, O. Heidrich, E. Olazabal, D. Geneletti, H. Orru, A.G. Bhave, N. Mittal, E. Feliu, and M. Faehnle. "Mitigating and Adapting to Climate Change: Multi-Functional and Multi-Scale Assessment of Green Urban Infrastructure." *Journal of Environmental Management* 146 (2014): 107–115. https://doi.org/10.1016/j.jenvman.2014.07.025.
[15] McFarland, A., L. Larsen, K. Yeshitela, A. N. Engida, and N. G. Love. "Guide for the Use of Green Infrastructure in Urban Environments for Stormwater Management." *Environmental Science: Water Research & Technology* 5, no. 4 (2019): 643–659. https://doi.org/10.1039/C8EW00498F.
[16] Xing, Yun, Huili Chen, Qiuhua Liang, and Xieyao Ma. “Improving the Performance of City-Scale Hydrodynamic Flood Modelling through a GIS-Based DEM Correction Method.” *Natural Hazards* 112 (2022): 2313–2335. https://doi.org/10.1007/s11069-022-05267-1.
[17] Cui, Yunsong, Qiuhua Liang, Gang Wang, Jiaheng Zhao, Jinchun Hu, Yuehua Wang, and Xilin Xia. “Simulation of Hydraulic Structures in 2D High-Resolution Urban Flood Modeling.” *Water* 11 (10) (2019): 2139. https://doi.org/10.3390/w11102139.
[18] Szymkiewicz, R. "Numerical Integration of the System of Saint Venant Equations." In *Numerical Modeling in Open Channel Hydraulics*, edited by Szymkiewicz, R., 301–365. Springer, 2009. https://doi.org/10.1007/978-90-481-3674-2_8.
[19] Lepelletier, T., and Q. Araud. "Implicit Formulation for 1D and 2D St Venant Equations—Presentation of the Method, Validation and Applications." In *Advances in Hydroinformatics*, edited by Gourbesville, P., J. Cunge, and G. Caignaert, 91–103. Springer, 2018. https://doi.org/10.1007/978-981-10-7218-5_6.
[20] Roohi, M., K. Soleymani, M. Salimi, and M. Heidari. "Numerical Evaluation of the General Flow Hydraulics and Estimation of the River Plain by Solving the Saint–Venant Equation." *Modeling Earth Systems and Environment* 6 (2020): 645–658. https://doi.org/10.1007/s40808-020-00718-9.
[21] Shayannejad, M., M. Ghobadi, and K. Ostad-Ali-Askari. "Modeling of Surface Flow and Infiltration During Surface Irrigation Advance Based on Numerical Solution of Saint–Venant Equations Using Preissmann's Scheme." *Pure and Applied Geophysics* 179 (2022): 1103–1113. https://doi.org/10.1007/s00024-022-02962-9.
[22] Koradia, A., and B. Barman. "Numerical Solution of Two-Dimensional Shallow Water Flow with Finite Difference Scheme." Paper presented at the 26th International Conference on Hydraulics, Water Resources and Coastal Engineering (HYDRO 2021), Surat, Gujarat, India, December 23-25, 2021. In *Fluid Mechanics and Hydraulics*, edited by Timbadiya, P. V., R. K. Ghosh, and S. K. Sinha. *Lecture Notes in Civil Engineering* 314 (2023): 115–126. https://doi.org/10.1007/978-981-19-9151-6_10.
[23] Jabbar, M., M. Mohd Yusoff, and A. Shafie. "Assessing the Role of Urban Green Spaces for Human Well-Being: A Systematic Review." *GeoJournal* 87 (2022): 4405–4423. https://doi.org/10.1007/s10708-021-10474-7.
[24] Magaña Rodríguez, D., E. Tudela Rivadeneyra, M. Meza Pérez, and A. Suárez Bonilla. "Green Infrastructure in Mexican Cities / Infraestructura Verde en Ciudades Mexicanas." Universidad Nacional Autónoma de México, 2021. https://repositorio.fa.unam.mx/bitstream/123456789/19063/1/Infraestructura_verde_en_ciudades_mexicanas.pdf.
[25] Fuentes-Mariles, Ó. A., J. Gracia-Sánchez, J. A. Chompa-Abarca, and F. De Luna-Cruz. "Predesign of an Urban Stormwater Drainage Network Using Genetic Algorithms / Prediseño de una red de drenaje

pluvial urbana con algoritmos genéticos." *Ingeniería, investigación y tecnología* 24, no. 2 (2023): 1-13. https://doi.org/10.22201/fi.25940732e.2023.24.3.021.
[26] Sañudo, E., L. Cea, and J. Puertas. "Modelling Pluvial Flooding in Urban Areas Coupling the Models Iber and SWMM." *Water* 12, no. 9 (2020): 2647. https://doi.org/10.3390/w12092647.
[27] Wang, S., J. Wang, K. Xin, H. Yan, S. Li, and T. Tao. "Urban Flood Modeling with a Novel Coupling Method of Surface and Sewer Hydrodynamic Processes." *Water Science & Technology* 89, no. 11 (2024): 3021–3034. https://doi.org/10.2166/wst.2024.172.
[28] Abdelrahman, Y. T., A. M. El Moustafa, and M. Elfawy. "Simulating Flood Urban Drainage Networks Through 1D/2D Model Analysis." *Journal of Water Management Modeling* 26 (2018): C454. https://doi.org/10.14796/JWMM.C454.
[29] Fan, Y., T. Ao, H. Yu, G. Huang, and X. Li. "A Coupled 1D–2D Hydrodynamic Model for Urban Flood Inundation." *Advances in Meteorology*, no. 1 (2017): Article ID 2819308. https://doi.org/10.1155/2017/2819308.
[30] Noh, S. J., J. Lee, S. Lee, K. Kawaike, and D. J. Seo. "Hyper-Resolution 1D–2D Urban Flood Modelling Using LiDAR Data and Hybrid Parallelization." *Environmental Modelling & Software* 103, no. C (2018): 131 - 145. https://doi.org/10.1016/j.envsoft.2018.02.008.